

# P59 High-frequency Dual-Doppler Analysis of a Retrograding Dryline/Baroclinic Boundary Intersection

Anthony E. Reinhart<sup>1\*</sup>, Christopher C. Weiss<sup>1</sup>, and David C. Dowell<sup>2</sup>

<sup>1</sup>Atmospheric Science Group, Department of Geosciences, Texas Tech University, Lubbock, TX

<sup>2</sup>NOAA/ESRL/GSD, Boulder, CO

## 1. INTRODUCTION

The dryline is a mesoscale gradient in dewpoint temperature that occurs during the spring and summer months over the southern Plains (Schaefer 1974; Schaefer 1986). The dryline separates a dry air mass originating from the elevated terrain of the desert southwest from a moist air mass originating from the Gulf of Mexico (Schaefer 1986). It typically propagates eastward along the sloped terrain of the High Plains during the morning and afternoon hours and retreats westward in the evenings and night when solar insolation weakens (Schaefer 1986). Drylines are commonly associated with the development of severe storms (Fujita 1958; Ogura and Chen 1977; Bluestein and Parker 1993; Weiss and Bluestein 2002), particularly during forward propagation.

When the dryline interacts with a baroclinic boundary the region of interaction is referred to as a triple point (Weiss and Bluestein 2002). The triple point is a favorable region for sustained convective initiation, during the day, because there is an increased amount of convergence and frontogenesis at this location (Berry and Bluestein 1982; Bluestein and Parker 1983; Weiss and Bluestein 2002).

The Texas Tech Atmospheric Science Group and Wind Science and Engineering

Research Center have developed two high frequency radars (TTUKa) that utilize the Ka frequency band (35 GHz) (Fig. 1) (Weiss et al. 2009). The high frequency coupled with a novel non-linear pulse compression technique allows the radars to have high sensitivity and a high spatial resolution ideal for sampling of fine-scale structures present in drylines and other clear air boundaries. Details of the radars can be found in Table 1.

## 2. EVENT SUMMARY

On 13 June 2010 the Verification of the Origin of Rotation in Tornadoes Experiment 2 (VORTEX2) armada was located in the Texas and Oklahoma panhandles intercepting a tornadic supercell that was initiated along the triple point between the dryline and a stalled outflow boundary. This intersection between the stalled outflow air mass and the dryline initiated convection for several hours throughout the afternoon and evening (Fig. 2).

Outflow from the complex of thunderstorms began to propagate southwestward towards Amarillo, TX. The propagation can be attributed to reinforcement of the aforementioned outflow air mass by convection. At the same time the dryline had reached its maximum eastward extent and begun to retreat westward around 0000 UTC on 14 June 2010. The intersection between the dryline and the convectively reinforced outflow air mass neared Amarillo, TX around 0220 UTC.

---

\* Corresponding author address: Anthony E. Reinhart, Texas Tech University, Atmospheric Science Group, Department of Geosciences, Lubbock, TX 79409; anthony.reinhart@ttu.edu

Following the collection of data on 13 June 2010 as part of VORTEX2, the two TTUKa radars sampled the dryline/baroclinic boundary intersection. During this time 37 full PPIs were collected (approximately 3 PPIs per minute). Ground clutter was an issue with this deployment so a one-degree elevation angle was used to minimize the effect of ground targets.

The TTUKa-1 radar was located at 35.25924 N and 101.62826 W and the TTUKa-2 radar was located at 35.27133 N and 101.54112 W, which is east of Amarillo, TX near US 60 and just east of the Amarillo airport. The 8 km long baseline extended east-to-west. The TTUKa-1 radar had a heading of 240 degrees and TTUKa-2 radar had a heading of 91.5 degrees. The triple point passed through the dual-Doppler lobe of the two TTUKa radars (Fig. 3) between 0222 UTC and 0232 UTC at a range of approximately 10 km. The two radars were oriented in an East-West fashion with the intersection point between the two boundaries propagating through the southern dual-Doppler lobe (Fig. 3).

### 3. METHODOLOGY

Radar data were processed using the SOLO program (Oye et al 1995). The radial velocities were thresholded to remove spurious values that correspond with ground clutter and with equivalent reflectivity values deemed too low to yield acceptable assigned velocities. The radial velocity fields were further cleaned up to remove any speckling that occurred. No dealising of the radial velocity field was necessary.

Objective analyses of the radar data were completed using the Observation Processing and Wind Synthesis (OPAWS) program. The data were projected onto a three-dimensional grid and then

processed using a two-pass Barnes analysis (Barnes 1964; Majcen et al. 2008). The two-pass Barnes scheme allows for the retention of smaller scales of motion, while still properly suppressing spurious wave features better than single pass methods (Barnes 1964; Koch et al. 1983; Trapp and Doswell 2000). Using a two-pass objective analysis technique provides greater precision in the analyses of gradients within the flow field, which are important in this study.

Recommendations from Koch et al. (1983), Pauley and Wu (1990), Trapp and Doswell (2000), and Majcen et al. (2008) were used to determine the horizontal grid point spacing,  $\kappa$  value, and  $\gamma$  value. The grid point spacing of 50 meters was calculated by determining the availability and spacing of data at the maximum range of dual-Doppler analysis as suggested in Koch et al. (1983). The grid stretches 12 km in the east-west direction and 9 km in the north-south direction. This domain encompasses the entire dual-Doppler time period. The smoothing parameter  $\kappa$  is  $0.033 \text{ km}^2$  and a  $\gamma$  of 0.30 was used for each radar.

Dual-Doppler synthesis was performed on the objectively analyzed data. The dual-Doppler code uses an iterative upward integration technique that assumes vertical velocity is equal to zero on the lateral edges of the domain. A minimum 30 degree crossing angle was used to minimize computational errors.

### 4. PRELIMINARY RESULTS

The high spatial resolution of the TTUKa radars provide a detailed look at the intersection between the dryline and the outflow boundary. In addition to the intersection zone that is present, the three air masses (dry environmental air (I), moist environmental air (II), and convectively reinforced outflow air (III))

remain distinctive throughout the dual-Doppler time period (Fig. 4).

The intersection misocyclone extends over an area approximately one kilometer in diameter (Fig. 5) as determined by the wind field. Over the ten minute period of dual-Doppler coverage, the intersection misocyclone remains approximately one kilometer in diameter while propagating westward over the analysis time period (Fig. 6). Isochrone analysis reveals the tendency of the dryline to bulge eastward just to the south of the intersection misocyclone, which is consistent with Buban et al. (2007) and Wakimoto and Murphey (2009).

Convergence within the intersection misocyclone ( $\sim 8 - 12 \times 10^{-2} \text{ s}^{-1}$ ) is no stronger than that found individually along the outflow boundary and the dryline (Fig. 7). In fact, the boundary between air masses I and III features stronger convergence ( $\sim 15 \times 10^{-2} \text{ s}^{-1}$ ) than that found at the triple point (Fig. 7).

## 5. FUTURE WORK

This study shows the advantage of the high sensitivity and resolution that the TTUKa radars provide, as applied to the fine-scale features of a triple point. This study will further look at the evolution of convergence and vertical vorticity associated with small eddies along the dryline and outflow boundary, especially as they interact with the triple point. The vertical velocity and convergence fields will be corroborated with RHIs taken of the triple point during the deployment.

## ACKNOWLEDGEMENTS

The authors would like to acknowledge Patrick Skinner and Scott Gunter for their helpful comments. Curtis Alexander for graciously sharing the DReader program.

This research was conducted under grant AGS-0964088 from the National Science Foundation.

## REFERENCES

- Barnes, S. L., 1964: A technique for maximizing details in numerical weather map analysis. *J. Appl. Meteor.*, 3, 396–409.
- Berry, E. K., and H. B. Bluestein, 1982: The formation of severe thunderstorms at the intersection of a dryline and a front: The role of frontogenesis. Preprints, 12th Conf. on Severe Local Storms, San Antonio, TX, Amer. Meteor. Soc., 597–602.
- Bluestein, H. B., and S. Parker, 1993: Modes of isolated, severe convective-storm formation along the dryline. *Mon. Wea. Rev.*, 121, 1354–1372.
- Buban, M. S., C. L. Ziegler, E. N. Rasmussen, Y. P. Richardson, 2007: The dryline on 22 May 2002 during IHOP: Ground-radar and in situ data analyses of the dryline and boundary layer evolution. *Mon. Wea. Rev.*, 135, 2473–2505.
- Fujita, T. T., 1958: Structure and movement of a dry front. *Bull. Amer. Meteor. Soc.*, 39, 574–582.
- Koch, S. E., M. desJardins, and P. J. Kocin, 1983: An interactive Barnes objective map analysis scheme for use with satellite and conventional data. *J. Climate Appl. Meteor.*, 22, 1487–1503.
- Majcen, M., P. Markowski, Y. Richardson, D. Dowell, J. Wurman, 2008: Multipass objective analyses of Doppler radar data. *J. Atmos. Oceanic Technol.*, 25, 1845–1858.
- Ogura, Y., and Y. Chen, 1977: A life

history of an intense mesoscale convective storm in Oklahoma. *J. Atmos. Sci.*, 34, 1458–1476.

Oye, R., C. K. Mueller, and S. Smith, 1995: Software for radar translation, visualization, editing, and interpolation. Preprints, 27<sup>th</sup> Conf. on Radar Meteorology, Vail, CO, Amer. Meteor. Soc., 359–361.

Pauley, P. M., and X. Wu, 1990: The theoretical, discrete, and actual response of the Barnes objective analysis scheme for one- and two-dimensional fields. *Mon. Wea. Rev.*, 118, 1145–1163.

Schaefer, J. T., 1974: The life cycle of the dryline. *J. Appl. Meteor.*, 13, 444–449.

-----, J. T., 1986: The dryline. *Mesoscale Meteorology and Forecasting*, P. S. Ray, Ed., Amer. Meteor. Soc., 549–572.

Trapp, R. J., C. A. Doswell, 2000: Radar data objective analysis. *J. Atmos. Oceanic Technol.*, 17, 105–120.

Wakimoto, R. M., Hanne V. Murphey, E. V. Browell, S. Ismail, 2006: The “triple point” on 24 May 2002 during IHOP. Part I: Airborne Doppler and LASE analyses of the frontal boundaries and convection initiation. *Mon. Wea. Rev.*, 134, 231–250.

Weiss, C. C., H. B. Bluestein, 2002: Airborne pseudo-dual Doppler analysis of a dryline-outflow boundary intersection. *Mon. Wea. Rev.*, 130, 1207–1226.

-----, C.C., J.L. Schroeder, J. Guynes, P.

Skinner, and J. Beck, 2009: The TTUKa mobile radar: Coordinated radar and in situ measurements of supercell thunderstorms during project VORTEX2. 34<sup>th</sup> AMS Radar Conference, Williamsburg, Virginia, October, 2009

Table 1: Specifications of the TTUKa radar system for VORTEX2 (Weiss et al. 2009).

Transmitter Frequency:	34,860 MHz
Transmit Power:	200 W peak
Transmitter Type:	TWTA
Duty Cycle:	Up to 50%
Antenna Gain:	50 dB
Antenna Type:	Cassegrain feed, epoxy reflector
Antenna Beamwidth:	0.49 degrees
Polarization:	Linear, horizontal
Waveguide:	WR-28, pressurized
PRF:	Variable up to 20 KHz
Gate Spacing:	15 m
Receiver:	MDS: -118 dBm
IF Frequency:	60 MHz
Pedestal:	Orbit AL-4016
DSP:	Sigmat RVP-8
Vehicle:	Chevy C550 Crewcab
Moments:	Reflectivity, radial velocity, spectrum width



Fig. 1: A photograph of the TTUKa-1 radar scanning a supercell near Greensburg, KS on 9 June 2009.

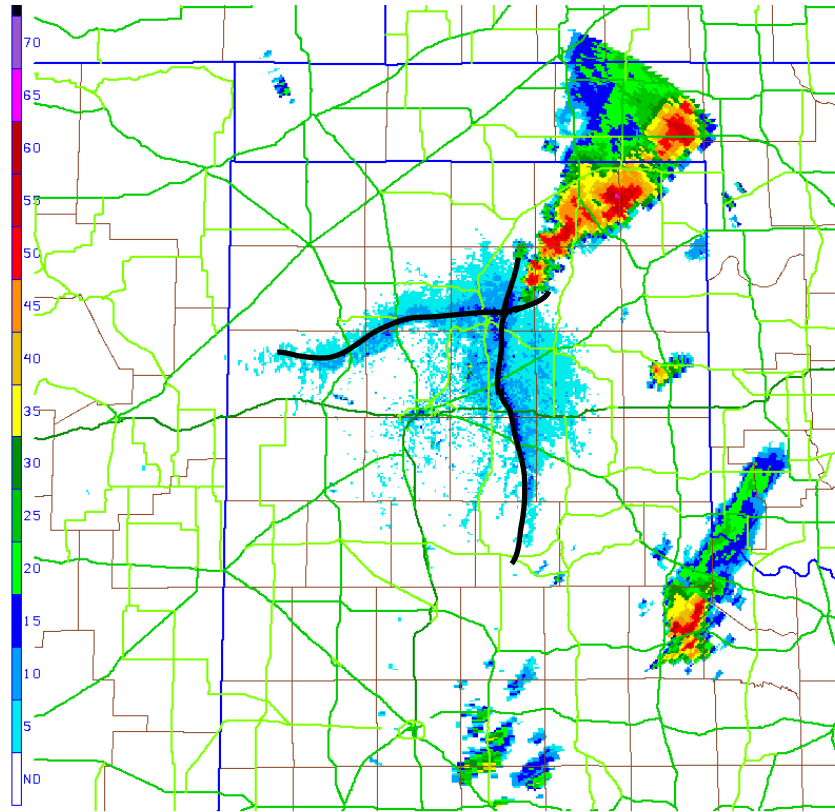


Fig. 2: Radar reflectivity from the Amarillo WSR-88D showing convection originating from the triple point at 2221 UTC. The black lines indicate the position of the dryline (roughly north-south) and baroclinic boundary (roughly east-west).

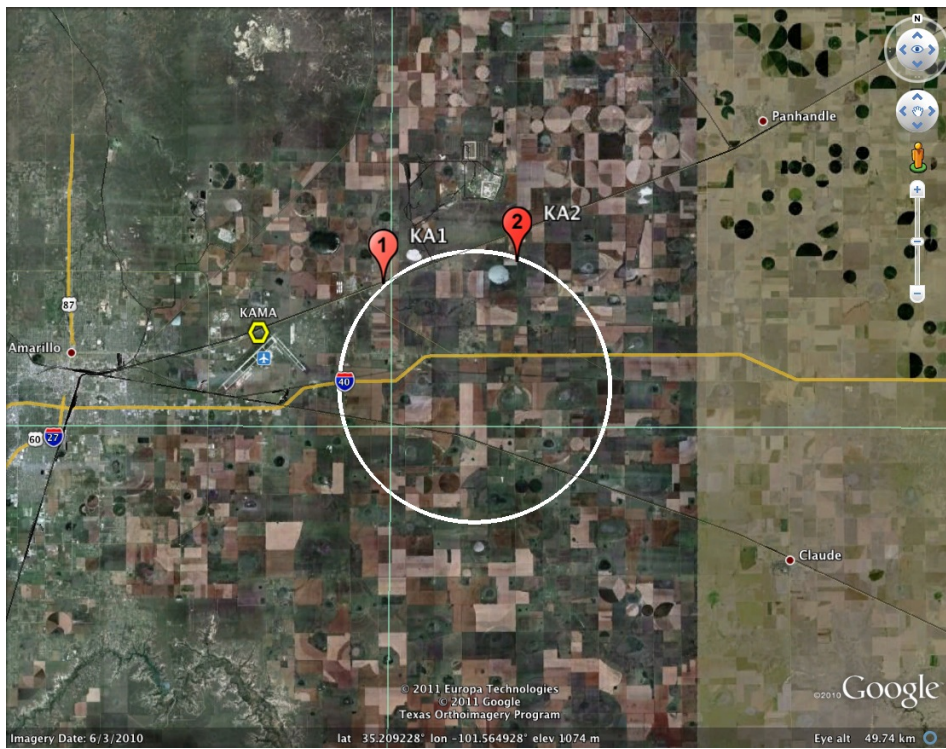


Fig. 3: Google Map image that shows the locations of the two TTUKa radars (red markers) with the Amarillo WSR-88D (yellow marker). The white circle is the location of the southern dual-Doppler lobe.

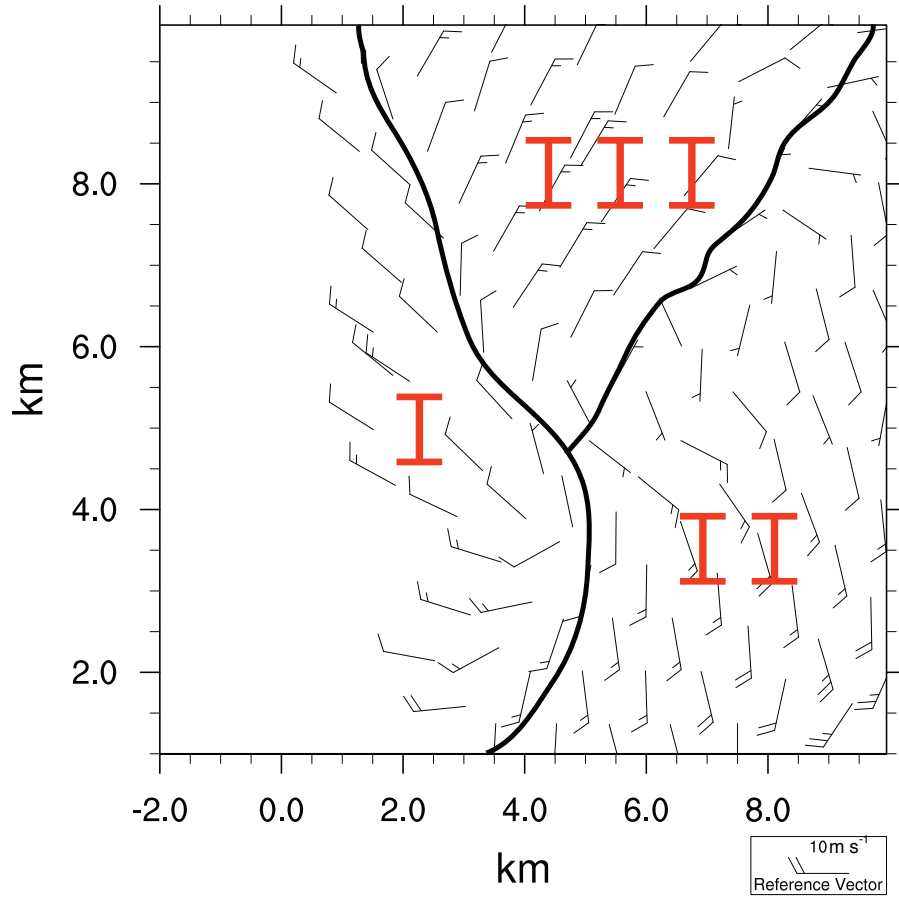


Fig. 4: Locations of the three different air masses overlaid on the dual-Doppler wind analysis. Air mass labeled I is the dry environmental air mass, air mass II is the moist environmental air mass, and air mass III is the convectively reinforced outflow air mass.

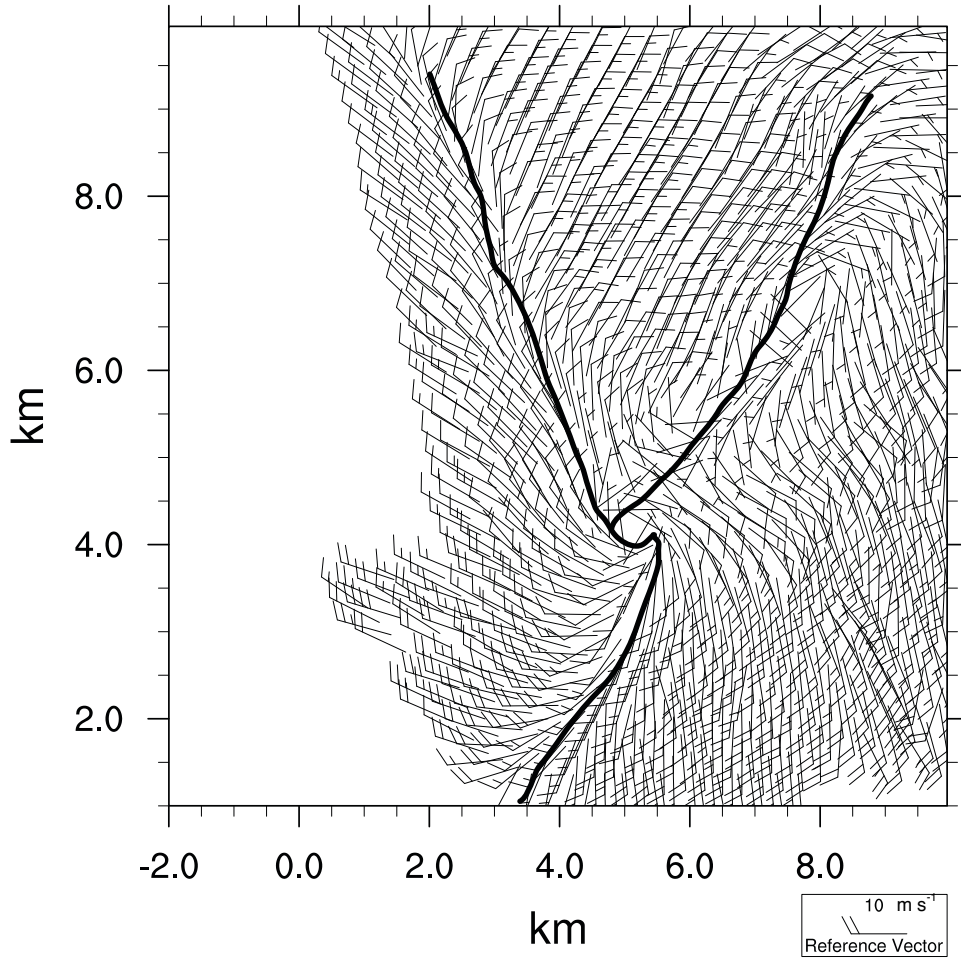


Fig. 5: Dual-Doppler analysis at 0222:47 UTC. The blue box indicates the intersection misocyclone or triple point. The black lines indicated the location of air mass boundaries.

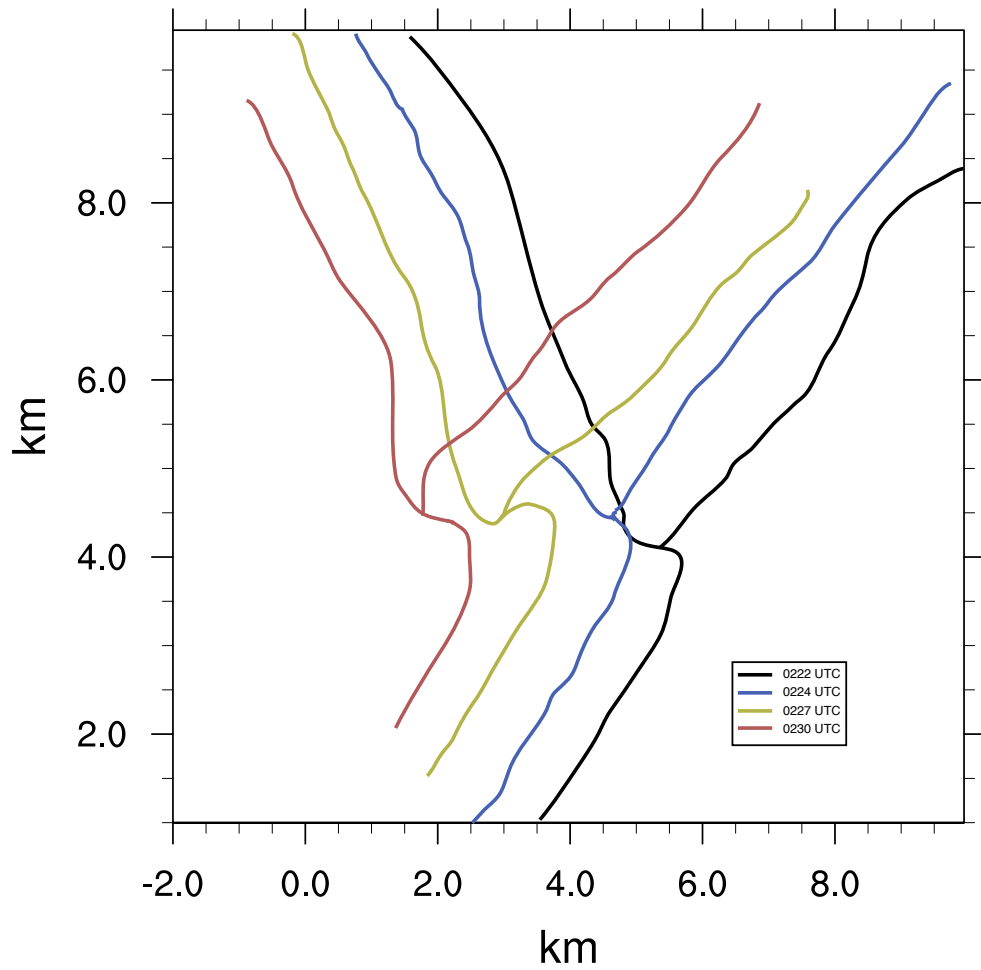


Fig. 6: Isochrone analysis of the air mass boundaries and triple point at 0222 UTC (black), 0224 UTC (blue), 0227 UTC (yellow), and 0230 UTC (red).

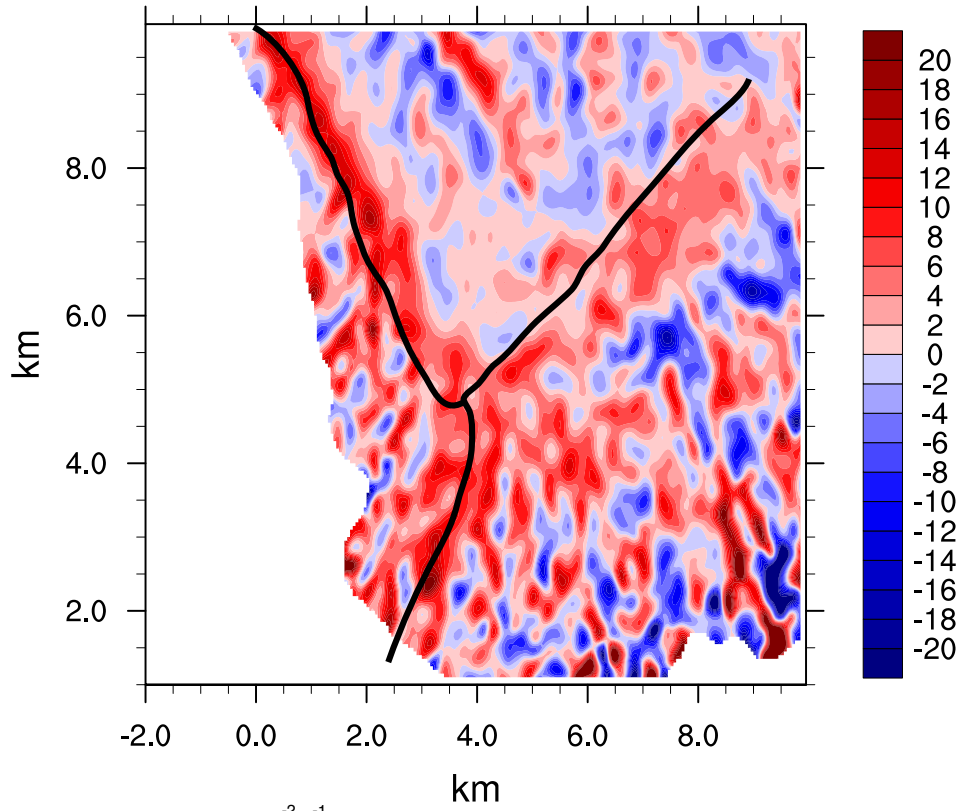


Fig. 7: Convergence (contoured,  $\times 10^{-2} \text{ s}^{-1}$ ) derived from the dual-Doppler analysis at 0226:16 UTC. The black lines indicate the location of the air mass boundaries.